Supporting Information

Synthesis of Scaly Sn_3O_4/TiO_2 Nanobelts Heterostructure for Enhanced UV-Visible Light Photocatalytic Activity

Guohui Chen‡[a], Shaozheng Ji‡[a], Yuanhua Sang[a], Sujie Chang[a], Pin Hao[a], Zhenhuan Zhao[a], Jerome Claverie[c], Hong Liu[a,b], Guangwei Yu[a]**

[a]State Key Laboratory of Crystal Materials, Shandong University, Jinan, Shandong 250100, China

[b]Beijing Institute of Nanoenergy and Nanosystems, Chinese Academy of Science, Beijing 100864, China.

[c]NanoQAM Research Center, Department of Chemistry, University of Quebec at Montreal, 2101 rue Jeanne-Mance, CP 8888, Montreal, Quebec H3C3P8, Canada.

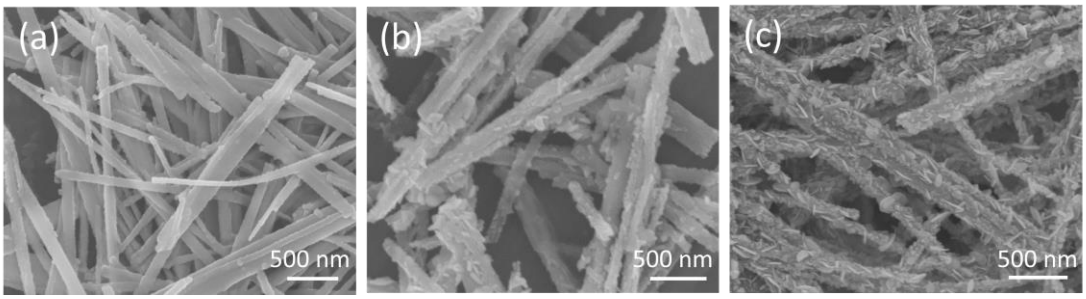

Figure S1. SEM images of scaly Sn_3O_4/TiO_2 (molar ratio Sn/Ti=2/1) heterostructure obtained at different synthetic stages of (a) 1 h; (b) 4 h; (c) 12 h.

To well understand the synthesis process of scaly Sn_3O_4/TiO_2 nanobelt heterostructure, morphology of the hybrid photocatalysts synthesized at 180 ℃ for different time was observed (Figure S1). Almost nothing can be observed at the surface of TiO_2 nanobelts for the sample obtained after a 1 hour hydrothermal treatment. Prolonging the reaction time to 4 h, many nanoparticles dispersed on the TiO_2 nanobelts can be found. When the reaction time is extended to 12 h, most of the nanoparticles have been converted into Sn_3O_4 nanoflakes. The images agree well with the prediction of synthetic process of the Sn_3O_4/TiO_2 heterostructure; 1) nucleation of Sn_3O_4

nanoparticles on the surface of the TiO_2 nanobelts, which is driven by the absorption of Sn^{2+} cations on -OH groups[1] on the surface coarsened TiO_2 nanobelts; (2) growth of Sn_3O_4 nuclei nanoflakes connected to TiO_2 lattice with a specific orientation.

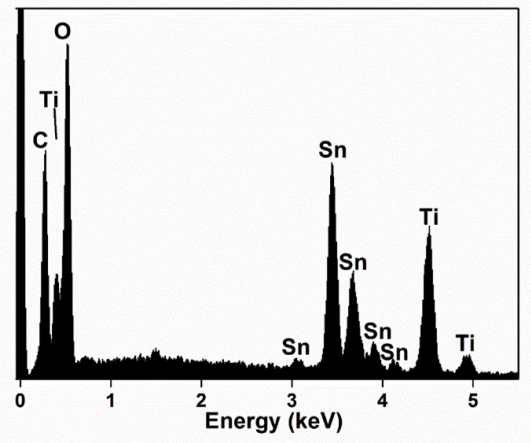

Figure S2. EDS analysis of the scaly Sn_3O_4/TiO_2 (molar ratio Sn/Ti=2/1) nanobelts heterostructure.

Figure S2 represents EDS analysis of the scaly Sn_3O_4/TiO_2 nanobelts heterostructure when the initial Sn/Ti molar ratio designed as 2/1, confirming the existence of Ti, Sn, O, and the weight ratio of Sn_3O_4 (52.5%).

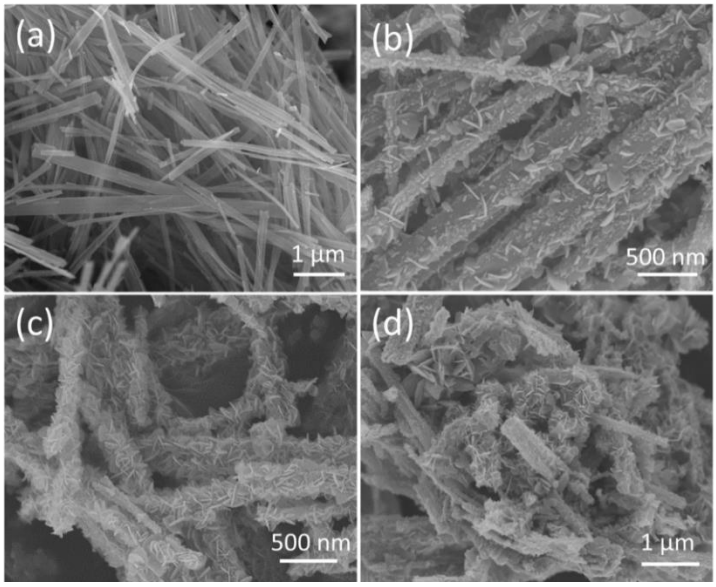

Figure S3. SEM images of (a) surface coarsened TiO_2 nanobelts; (b) Sn_3O_4/TiO_2 (molar ratio Sn/Ti=1/1) heterostructure; (c, d) Sn_3O_4/TiO_2 (molar ratio Sn/Ti=3/1) heterostructure of different magnification

Sn_3O_4/TiO_2 with different initial Sn/Ti molar ratios of 1/1 and 3/1 were conducted and their SEM images are presented in Figure S3b-d. Similar hierarchical TiO_2 nanobelts structures with less heterojunctional density are observed when Sn/Ti is 1/1. When the Sn/Ti molar ratio is 3/1, the Sn_3O_4 flakes cover almost completely the TiO_2 nanobelts and excessive nanoflakes gathered into aggregates are absorbed at the surface of the nanobelts.

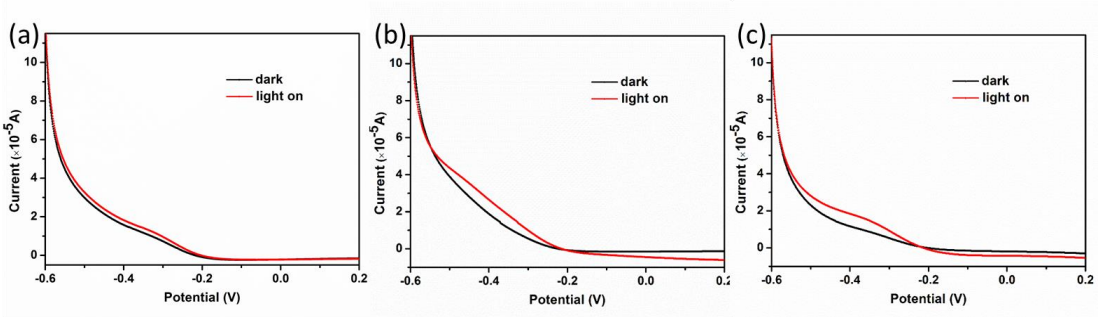

Figure S4. Current-potential (*I-V*) characteristics of (a) TiO_2 nanobelt; (b) Sn_3O_4 nanoflakes; (c) the Sn_3O_4/TiO_2 (molar ratio Sn/Ti=2/1) nanobelts heterostructure at applied bias from -0.6 to 0.2 V under dark (black line) and simulated solar spectrum irradiation (red line).

Figure S4 shows I-V curves of Sn_3O_4, TiO_2 and Sn_3O_4/TiO_2 (molar ratio Sn/Ti=2/1) heterostructure. The high dark currents of Sn_3O_4 and Sn_3O_4/TiO_2 was determined by the applied bias voltage of -0.35 V, the corresponding dark current for TiO_2, Sn_3O_4 and Sn_3O_4/TiO_2 was about 11.5 μA, 12.9 μA, and 11.1 μA, respectively. The reason for the decrease currents at more positive voltage was probably that the bias potential not sufficient to produce electric field to favor separation of photoexcited chargers.[3]

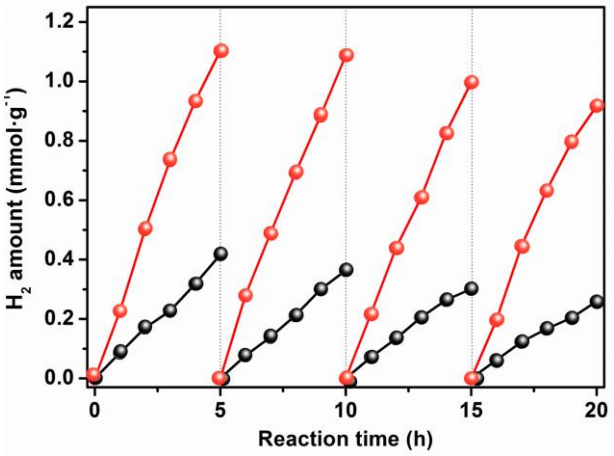

Figure S5. Cycle H_2 evolution of Sn_3O_4/TiO_2-2 heterostructure as a function of time with (red line) and without (black line) 1 wt % Pt co-catalyst under irradiation of the 300W Xe arc lamp.

Figure S5 compared the photocatalytic stability of Sn_3O_4/TiO_2-2 heterostructure with and without Pt as co-catalyst, after photo-deposited 1 wt % Pt, the Sn_3O_4/TiO_2-2 heterostructure exhibited a higher average hydrogen evolution rate of 218.7 $\mu mol \cdot h^{-1} \cdot g^{-1}$. Furthermore, the rate of hydrogen evolution dropped by a mere 20% after the fourth reaction cycle (20 h) without renewing the sacrificial agents (Figure S5 black line), and about 18.2% decrease with 1 wt % Pt as co-catalyst Figure S5 red line), indicating a good cyclability for the Sn_3O_4/TiO_2-2 heterostructure. The hydrogen evolution rate of TiO_2 nanobelts with 1wt % Pt as co-catalyst was 127.3 $\mu mol \cdot h^{-1} \cdot g^{-1}$, which was higher than that of Sn_3O_4 (102.2 $\mu mol \cdot h^{-1} \cdot g^{-1}$). This is mainly because TiO_2 has a higher density of states (DOS) in its unique *d*-orbital conduction band, which showed better hot-electron-accepting ability in the TiO_2-Pt Schottky barrier.[4] The good hydrogen evolution activity of Sn_3O_4/TiO_2-Pt (218.7 $\mu mol \cdot h^{-1} \cdot g^{-1}$) further indicate the leading effect of heterostructure between Sn_3O_4 and TiO_2 that greatly promote the separation and transfer of photoexcited charges. The existence of Sn ions in the solution are detected via adding NaOH to the solution. Precipitates were not observed during the experiment, indicating there was no or negligible Sn ions in the solution.

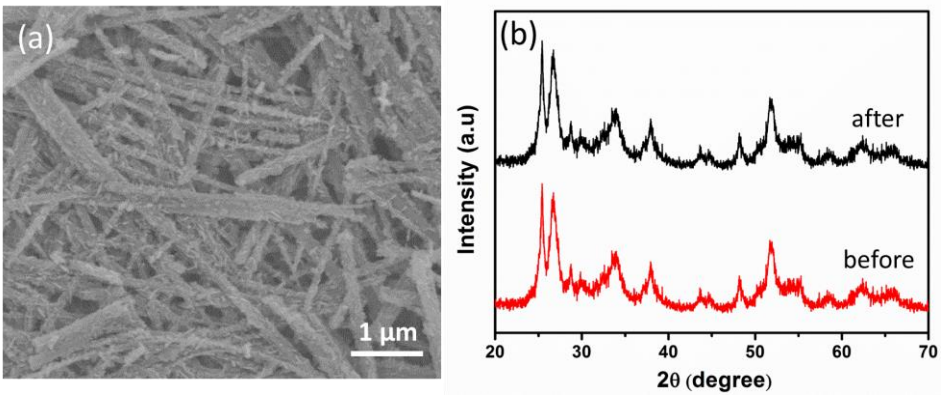

Figure S6. (a) SEM image of scaly Sn_3O_4/TiO_2 (molar ratio Sn/Ti=2/1) nanobelts heterostructure after hydrogen evolution; (b) XRD patterns of the Sn_3O_4/TiO_2 heterostructure before (red curve) and after (black curve) hydrogen evolution.

Based on the SEM image and XRD data above, we can conclude that morphology and crystal structure of the nanocomposites are visibly not affected by the hydrogen evolution.

Table S1. The BET specific surface areas of different samples.

Sample	Specific surface area ($m^2 \cdot g^{-1}$)
Surface coarsened TiO_2 nanobelts	38.591
Sn_3O_4 naoflakes	43.128
Scaly Sn_3O_4/TiO_2 nanobelts heterostructures	51.549

The Sn_3O_4/TiO_2-2 heterostructure display a larger specific surface area (51.5 $m^2 \cdot g^{-1}$) than single Sn_3O_4 nanoflakes (about 43.1 $m^2 \cdot g^{-1}$) (Table S1) and single surface coarsened TiO_2 nanobelts (38.6 $m^2 \cdot g^{-1}$),[2] the increased specific surface area can be result from the fabrication of Sn_3O_4/TiO_2 hierarchical nanostructures, as SEM and TEM images (Figure 2d and Figure 3c) show, Sn_3O_4 nanoflakes extended the surface area of TiO_2 by growing along the 1D TiO_2 nanobelts. While single Sn_3O_4 sample would likely to gather into aggregates.

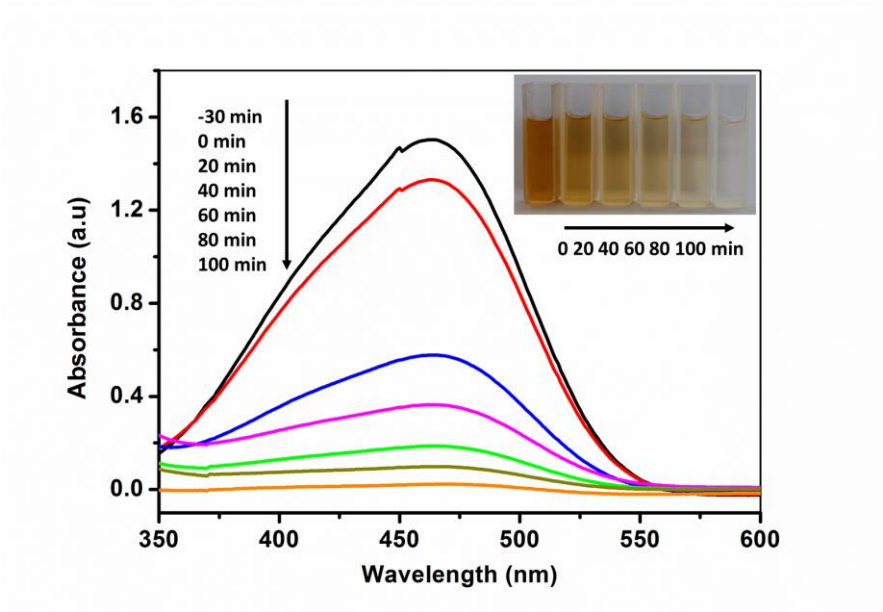

Figure S7. Typical UV-vis spectra and photographs (up right inset) of methyl orange solution at different simulated solar spectrum irradiation time intervals by using Sn_3O_4/TiO_2 (molar ratio Sn/Ti=2/1) nanobelts heterostructure as photocatalyst.

The degradation of MO dye was used to assess the photodegradation ability of the photocatalysts. The concentration of MO at time t and time t =0, was measured by its optical absorbance at 465 nm (Figure S7). The high degradation efficient in the initial 20 minutes was partially because of the absorption of MO during the adsorption-desorption equilibrium and the kinetic process of photocatalysis.[5]

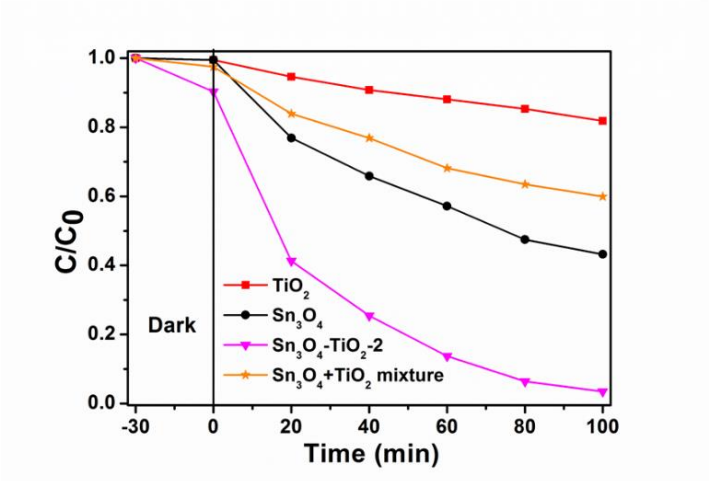

Figure S8. Photodegradation activity of physical mixture sample that composed of 47.5 wt% TiO_2 and 52.5 wt% Sn_3O_4 in comparison with TiO_2, Sn_3O_4, and Sn_3O_4/TiO_2-2 heterostructure under simulated solar spectrum irradiation.

Photocatalytic activity of the physical mixture of 47.5 wt% TiO_2 nanobelts and 52.5 wt% Sn_3O_4 nanoflakes that in agreement with the component of Sn_3O_4/TiO_2-2 heterostructure as indicated by EDS, was measured under simulated solar spectrum irradiation. As shown in Figure S8, the degradation rate of the physical mixture sample was much lower than Sn_3O_4/TiO_2-2 heterostructure, also proved the heterojunction plays a positive role in photoexcited charge transfer and separation.

References

1 J. F. Reeves, S. J. Davies, N. J. Dodd and A. N. Jha, *Mutation Research/Fundamental and Molecular Mechanisms of Mutagenesis*, 2008, 640, 113-122.

2 J. Tian, Y. Sang, Z. Zhao, W. Zhou, D. Wang, X. Kang, H. Liu, J. Wang, S. Chen, H. Cai and H. Huang, *Small*, 2013, 9, 3864-3872.

3 J. H. Sohn, H. G. Cha, C. W. Kim, D. K. Kim and Y. S. Kang, *Nanoscale*, 2013, **5**, 11227-11233.

4 C. Clavero, *Nature Photonics*, 2014, **8**, 95-103.

5 N. Barka, S. Qourzal, A. Assabbane and Y. Ait-Ichou, *Journal of Environmental Science and Engineering*, 2010, **4**, 1-5.